

Numerical Heat Transfer, Part A: Applications

An International Journal of Computation and Methodology

ISSN: (Print) (Online) Journal homepage: <https://www.tandfonline.com/loi/unht20>

Impacts of uniform and sinusoidal heating in a nanofluid saturated porous chamber influenced by the thermal radiation and the magnetic field

S. Muthukumar, S. Sureshkumar, Shreen El-Sapa & Ali J. Chamkha

To cite this article: S. Muthukumar, S. Sureshkumar, Shreen El-Sapa & Ali J. Chamkha (2022): Impacts of uniform and sinusoidal heating in a nanofluid saturated porous chamber influenced by the thermal radiation and the magnetic field, Numerical Heat Transfer, Part A: Applications, DOI: [10.1080/10407782.2022.2137072](https://doi.org/10.1080/10407782.2022.2137072)

To link to this article: <https://doi.org/10.1080/10407782.2022.2137072>



Published online: 03 Nov 2022.



Submit your article to this journal [↗](#)



Article views: 71



View related articles [↗](#)



View Crossmark data [↗](#)



Impacts of uniform and sinusoidal heating in a nanofluid saturated porous chamber influenced by the thermal radiation and the magnetic field

S. Muthukumar^a, S. Sureshkumar^b, Shreen El-Sapa^c, and Ali J. Chamkha^d

^aDepartment of Mathematics, K. S. Rangasamy College of Technology, Tiruchengode, Tamil Nadu, India;

^bDepartment of Mathematics, Kongu Engineering College, Erode, Tamil Nadu, India; ^cDepartment of Mathematical Sciences, College of Science, Princess Nourah Bint Abdulrahman University, Riyadh, Saudi Arabia; ^dFaculty of Engineering, Kuwait College of Science and Technology, Doha

ABSTRACT

A numerical investigation on the impacts of heater length increased from left corner along with the bottom wall in a Cu-water nanofluid-filled porous cavity in the existence of MHD and thermal radiation is performed out. The bottom wall is heated with two different types of heater (both uniform and nonuniform) separately. Three various lengths of heater are considered. Constant cold upper horizontal wall moves in the positive direction. The other sidewalls and excluding the heating portion of the bottom wall are considered to be adiabatic. The system of dimensionless form of governing equations is solved by finite volume method (FVM) with appropriate boundary and initial conditions and SIMPLE algorithm has been employed for the pressure term. For both types of heating, the highest heat transfer is attained with the length of heater $L_H = 1/4$ for all taken Richardson number. The effect of magnetic field is very low on heat transfer with the thermal source length $L_H = 1/2$ and nonuniform heating in free convection regime. On increasing the heater length in nonuniform heating, overall heat transfer rate is decreased first and then raised. The percentage of increasing of average Nusselt number with an increase of thermal radiation parameter in nonuniform heating is higher than uniform heating. The effect of magnetic field is significant for all taken solid volume fraction in uniform heating than the nonuniform heating with heater length $L_H = 1/2$.

ARTICLE HISTORY

Received 17 August 2022

Revised 19 September 2022

Accepted 11 October 2022

KEYWORDS

MHD; mixed convection; nanofluid; porous cavity; sinusoidal heating; thermal radiation

1. Introduction

The activities of fluid particles of electrically conducting fluid with the power of electromagnetic field, Magneto-Hydrodynamics (MHD), are one of the most important problems in several engineering applications such as crystal growth, cooling of nuclear reactors, and plasma confinement. Many researchers have made a discussion on MHD convection in an enclosure. Also, the position of heat source plays a vital role in convective heat transfer problems. Particularly, the location of heater at the bottom corner of the cavity is focused mainly by several researchers due to its occurrences in many engineering applications. Oztop et al. [1] reported on combined convection in an enclosure with partial heating in the presence of magnetic field. Dawood and Teamah [2] investigated the effects of double diffusive in a cavity in the existence of magnetic field. Also, Ray and Chatterjee [3], Malleswaran and Sivasankaran [4], and Selimefendigil and Chamkha [5]

Nomenclature

B_0	magnetic field	Greek	
C_p	specific heat	α	thermal diffusivity
Da	darcy number	β	thermal expansion coefficient
d_p	average particle size	$\Delta\theta$	temperature difference
F	Forchheimer coefficient	ϵ	porosity
g	gravitational acceleration	η	ratio of thermal conductivity of nano-layers
Gr	Grashof number	μ	dynamic viscosity
H	enclosure length	ν	kinematic viscosity
Ha	Hartmann number	ρ	density
h_{nl}	thickness of nano-layer	σ	electrical conductivity
K	permeability	θ	temperature
k	thermal conductivity	ϕ	phase deviation
L_H	length of heater	χ	solid volume fraction
Nu_{avg}	average Nusselt number	ω	ratio of the thickness of nano-layer
Nu	local Nusselt number	Subscripts	
p	fluid pressure	avg	average
P	dimensionless pressure	c	cold wall
Pr	Prandtl number	eff	effective
r_s	radius of nanoparticles	eq	equivalent
R	thermal radiation parameter	f	fluid
Re	Reynolds number	h	hot wall
Ri	<i>Richardson number</i>	l	left wall
T	dimensionless temperature	nf	nanofluid
u	velocity vector	nl	nano-layer
U, V	dimensionless velocities in X- and Y-direction respectively	o	reference state
u, v	velocities in x - and y -direction respectively	s	solid
U_0	lid velocity	r	right wall
X, Y	dimensionless Cartesian coordinates	Abbreviations	
x, y	Cartesian coordinates	CW	clockwise
		CCW	counterclockwise

studied the problem of MHD convection in a lid-moving chamber in different aspects. The common findings of their study are an increase of Hartmann number decreases the average Nusselt number and the magnetic field strongly affects the flow characteristics and heat transfer mechanism. Some other studies related to mixed convection in a lid-driven cavity with different geometries were performed [6,7]. Nanofluids, suspension of nanometer-sized solid particles into the base fluid, introduced by Choi and Eastman [8], are used instead of conventional fluids in heat transfer analysis for the past two decades due to its enhanced thermal conductivity. It is used in the fields of advanced nuclear systems, biomedicine, and food storage processing, etc., and many research works on nanofluids have been reported in the literature. The properties of nanofluid, thermal conductivity and viscosity, are experimentally verified [9,10]. Esfe et al. [11] studied convection in a nanofluid-filled cavity with moving lids. Their results suggested that an increase of the concentration of nanoparticles increases the heat transfer rate. The problem of convection in a rectangular cavity filled with nanofluid was discussed by Salahi et al. [12]. Some other works related to heat transfer of nanofluid in different cavities were performed [13–16]. It was confirmed that an increase in solid volume fraction of the nanoparticles increases the average Nusselt number.

Convection in porous media is one of the important problems in the fields of oil extraction, float glass production, and metal coating, etc. Irwan et al. [17] proposed a numerical study on fluid flow in a lid-driven chamber filled with fluid-saturated porous medium. It was found that

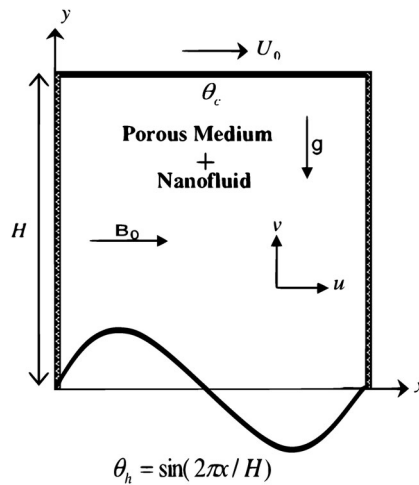


Figure 1. A schematic view of the physical model of the considered cavity.

the porosity of the media affects the velocity and behavior of the fluid in the enclosure significantly. Ramakrishna et al. [18] reported the effects of thermal aspect ratio and thermal boundary conditions in a porous square cavity. Their results revealed that forced convection dominates at low Darcy number whereas free convection dominates at high Darcy number. Also, Wang and Qin [19] discussed a problem on convective heat transfer of porous media with the effect of double-diffusive. Mansour et al. [20] studied the impacts of the magnetic field in a porous chamber saturated with gyrotactic microorganisms. Thermal radiation plays a vital role in designing the systems in engineering applications. Many researchers have included the effect of thermal radiation in their investigations. For example, the problems of impacts of radiation effect in a porous chamber filled with different fluids and thermal sources are discussed in [21–23]. Bibi et al. [24] performed a numerical modeling on heat transfer of Williamson fluid in the presence of thermal radiation and MHD. Recently, Ray et al. [25] studied the problem of convective flow of non-homogeneous fluid in a vertical plate with the effect of non-Fourier thermal relaxation.

Recently, researchers have focused on the problem of combined effect of nanofluid and porous medium in heat transfer analysis. Javed et al. [26] discussed the Lorentz force effect in a triangular porous cavity filled with micropolar fluid. Babazadeh et al. [27] studied the effects of nanoparticles shape in a porous medium in the presence of the magnetic field. Riaz et al. [28] analyzed the problem on the peristaltic propulsion of fluid flow through a porous symmetrical duct. Aly et al. [29] applied the ISPH method to analyze the heat transfer characteristics of nanofluid in a porous cavity. They observed that, in a porous cavity, an increase of solid volume fraction of nanofluid increases the average Nusselt number.

Based on the above survey of the literature, combining all the problems, such as convective heat transfer of MHD, nanofluid, porous medium and the effect of thermal radiation with sinusoidal partial heating is not carried out yet. This present investigation focuses on the impact of thermal radiation and MHD in a 2-D porous square cavity filled with nanofluid. Further, it includes the effect of partial or full heating of bottom wall with uniform or sinusoidal heating. When dispersing the nanoparticles into a base fluid, a layer around the nanoparticles is formed by the liquid molecules. This layer plays a major role in convective heat transfer of nanofluid. Many researchers have not considered this effect in their research. By applying the modified Maxwell model [30] for the effective thermal conductivity, we included it in this research. Additionally in this research, convection terms are expressed by employing the third-order accurate deferred QUICK scheme of Hayase et al. [31] which is more stable than the other schemes for solving conservation equations by finite volume method (FVM).

Table 1. Thermophysical properties of water and nanoparticles [12,29].

	$\rho(\text{kgm}^{-3})$	$C_p(\text{Jkg}^{-1}\text{K}^{-1})$	$k(\text{Wm}^{-1}\text{K}^{-1})$	$\beta \times 10^{-5}(\text{K}^{-1})$
Water	997.1	4,179	0.613	21
Copper Cu	8,933	385	401	1.67

2. Mathematical formulation

A 2-D, steady, and laminar flow is considered inside a porous cavity, which is depicted in Figure 1. The side lengths of the cavity are equal to H . The velocity components (u , v) with directions along the Cartesian coordinates (x , y) are shown in Figure 1. Water-copper (Cu) spherical nanoparticles fill the cavity. The fluid is assumed to be incompressible and non-Newtonian. It is assumed that the effect of Joule heating and viscous dissipation is negligible in the entire system. Two different types of thermal source, uniform and nonuniform with various lengths and constant temperature θ_h , are considered along the bottom wall. The lengths of heaters are $L_H = H/4$, $H/2$, H and it is extended from left to right. Constant cold upper horizontal wall with temperature θ_c moves in the positive direction with the speed of U_0 . The remaining sidewalls and excluding the heating portion of the bottom wall is taken as thermally insulated. A uniform magnetic field is applied in the horizontal direction with magnitude B_0 . Due to the Boussinesq approximation, the properties of the nanofluid (see Table 1) are not varied excluding the density. The impact of induced magnetic field and internal heat generation is not considered. The fluid particles are in thermally equilibrium with Cu particles and the slip velocity does not exist between fluid and nanoparticles. Characteristics of the porous medium are thermally isotropic, hydrodynamic, and locally thermally equilibrium with solid matrix. Radiation heat flux inside the cavity is described by Rosseland approximation [23]. The dimensional form of governing equations for the above assumptions are as follows [22,29]

$$\frac{\partial u}{\partial x} + \frac{\partial v}{\partial y} = 0 \quad (1)$$

$$\frac{u}{\epsilon} \frac{\partial u}{\partial x} + \frac{v}{\epsilon} \frac{\partial u}{\partial y} = -\frac{\epsilon}{\rho_{nf}} \frac{\partial p}{\partial x} + \frac{\mu_{nf}}{\rho_{nf}} (\nabla^2 u) - \frac{\mu_{nf}}{\rho_{nf}} \frac{\epsilon}{K} u - \frac{F}{K^{\frac{1}{2}}} \epsilon u \sqrt{u^2 + v^2} \quad (2)$$

$$\begin{aligned} \frac{u}{\epsilon} \frac{\partial v}{\partial x} + \frac{v}{\epsilon} \frac{\partial v}{\partial y} = & -\frac{\epsilon}{\rho_{nf}} \frac{\partial p}{\partial y} + \frac{\mu_{nf}}{\rho_{nf}} (\nabla^2 v) - \frac{\mu_{nf}}{\rho_{nf}} \frac{\epsilon}{K} v - \frac{F}{K^{\frac{1}{2}}} \epsilon v \sqrt{u^2 + v^2} \\ & + \frac{(\rho\beta)_{nf}}{\rho_{nf}} \epsilon g(\theta - \theta_c) - \frac{\sigma_{nf}}{\rho_{nf}} \epsilon B_0^2 v \end{aligned} \quad (3)$$

$$u \frac{\partial \theta}{\partial x} + v \frac{\partial \theta}{\partial y} = \frac{k}{(\rho C_p)_{nf}} \left(\frac{\partial^2 \theta}{\partial x^2} + \frac{\partial^2 \theta}{\partial y^2} \right) - \frac{1}{(\rho C_p)_{nf}} \left(\frac{\partial q_{rx}}{\partial x} + \frac{\partial q_{ry}}{\partial y} \right) \quad (4)$$

along with the boundary conditions:

$$u = U_0, v = 0, \quad \theta = \theta_c, \quad y = H$$

$$u = v = 0, \quad \frac{\partial \theta}{\partial x} = 0, \quad x = 0$$

$$u = v = 0, \quad \frac{\partial \theta}{\partial x} = 0, \quad x = H$$

$$u = v = 0, \quad y = 0$$

Case (i): $\theta = \theta_h(or)\theta = \sin\left(\frac{2\pi x}{H}\right)$, $0 \leq x \leq H/4$, $y = 0$

$$\frac{\partial \theta}{\partial y} = 0, \quad H/4 \leq x \leq H, y = 0$$

Case (ii): $\theta = \theta_h(or)\theta = \sin\left(\frac{2\pi x}{H}\right)$, $0 \leq x \leq H/2$, $y = 0$

$$\frac{\partial \theta}{\partial y} = 0, \quad H/2 \leq x \leq H, y = 0$$

Case (iii): $\theta = \theta_h(or)\theta = \sin\left(\frac{2\pi x}{H}\right)$, $0 \leq x \leq H$, $y = 0$

where K the permeability and F Forchheimer's coefficient can be written as follows

$$K = \frac{\epsilon^2 d_p^2}{a(1-\epsilon)^2}; \quad F = \frac{b}{\sqrt{a}\epsilon^{3/2}}$$

where $a = 150$ and $b = 1.75$ are Ergun's [32] constants and d_p stands for the average particle size of the bed.

The radiant flux is estimated by Rosseland diffusion approximation

$$q_{rx} = -\frac{4\sigma^*}{3k^*} \frac{\partial T^4}{\partial x}, \quad q_{ry} = -\frac{4\sigma^*}{3k^*} \frac{\partial T^4}{\partial y}$$

Eqs. (1)–(4) are converted into non-dimensional form by using the following dimensionless parameters:

$$X = \frac{x}{H}, \quad Y = \frac{y}{H}, \quad U = \frac{u}{U_0}, \quad V = \frac{v}{U_0}, \quad T = \frac{\theta - \theta_c}{\theta_h - \theta_c}, \quad Gr = \frac{g\beta\Delta\theta H^3}{\nu_f^2}, \quad Da = \frac{K}{H^2}, \quad Ha = B_0 H \sqrt{\frac{\sigma_f}{\mu_f}}, \quad R = \frac{4\sigma^* T_c^3}{kk^*},$$

$$P = \frac{p}{\rho U_0^2}, \quad Re = \frac{U_0 H}{\nu_f}, \quad Pr = \frac{\nu_f}{\alpha_f} \text{ and } Ri = \frac{Gr}{Re^2}.$$

Thus, the dimensionless form of the governing equations can be written as follows:

$$\frac{\partial U}{\partial X} + \frac{\partial V}{\partial Y} = 0, \quad (5)$$

$$\frac{1}{\epsilon^2} \left(U \frac{\partial U}{\partial X} + V \frac{\partial U}{\partial Y} \right) = -\frac{\rho_f}{\rho_{nf}} \frac{\partial P}{\partial X} + \frac{\mu_{nf}}{\epsilon Re \rho_{nf} \nu_f} (\nabla^2 U) - \frac{\mu_{nf}}{\rho_{nf} \nu_f} \frac{U}{Re Da} - \frac{1.75}{\sqrt{150}} \frac{(U^2 + V^2)^{1/2}}{\sqrt{Da}} \frac{U}{\epsilon^{3/2}} \quad (6)$$

$$\frac{1}{\epsilon^2} \left(U \frac{\partial V}{\partial X} + V \frac{\partial V}{\partial Y} \right) = -\frac{\rho_f}{\rho_{nf}} \frac{\partial P}{\partial Y} + \frac{\mu_{nf}}{\epsilon Re \rho_{nf} \nu_f} (\nabla^2 V) - \frac{\mu_{nf}}{\rho_{nf} \nu_f} \frac{V}{Re Da} - \frac{1.75}{\sqrt{150}} \frac{(U^2 + V^2)^{1/2}}{\sqrt{Da}} \frac{V}{\epsilon^{3/2}} + \frac{(\rho\beta)_{nf}}{\rho_{nf} \beta_f} (RiT) - \frac{\rho_f}{\rho_{nf}} \frac{\sigma_{nf}}{\sigma_f} \frac{(Ha)^2 V}{Re} \quad (7)$$

$$U \frac{\partial T}{\partial X} + V \frac{\partial T}{\partial Y} = \frac{\alpha_{nf}}{\alpha_f} \frac{1}{Pr \cdot Re} \left(1 + \frac{4}{3} R \right) \left(\frac{\partial^2 T}{\partial X^2} + \frac{\partial^2 T}{\partial Y^2} \right) \quad (8)$$

The appropriate boundary conditions are as follows:

$$U = 1, V = 0 \quad T = 0, \quad Y = 1$$

$$U = V = 0 \quad \frac{\partial T}{\partial X} = 0, \quad X = 0$$

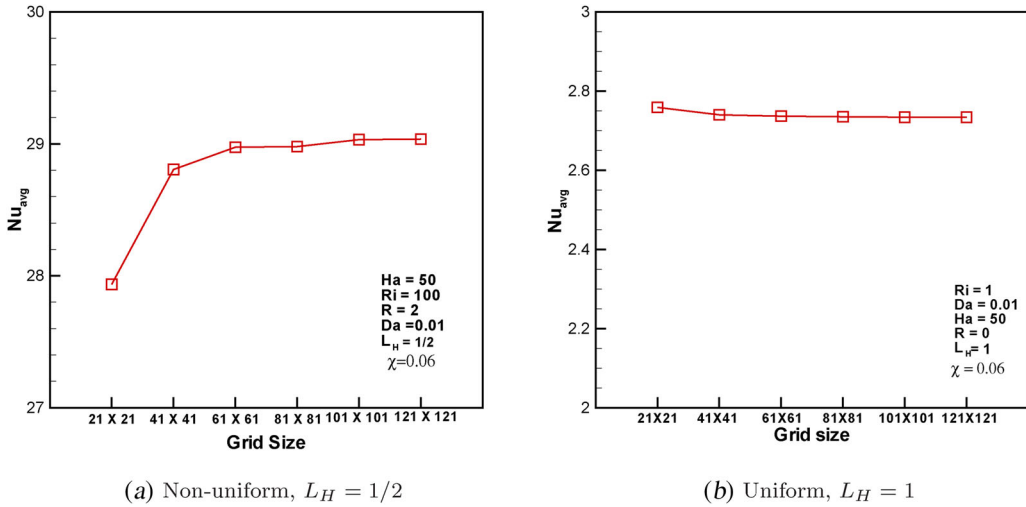


Figure 2. Average Nusselt numbers for different mesh sizes at $Ha = 50$, $Da = 10^{-2}$, and $\chi = 0.06$.

$$U = V = 0, \quad \frac{\partial T}{\partial X} = 0, \quad X = 1$$

$$U = V = 0, \quad Y = 0$$

Case (i): $T = 1$ (or) $T = \sin(2\pi X)$, $0 \leq X \leq 1/4$, $Y = 0$

$$\frac{\partial T}{\partial Y} = 0, \quad 1/4 \leq X \leq 1, \quad Y = 0$$

Case (ii): $T = 1$ (or) $T = \sin(2\pi X)$, $0 \leq X \leq 1/2$, $Y = 0$

$$\frac{\partial T}{\partial Y} = 0, \quad 1/2 \leq X \leq 1, \quad Y = 0$$

Case (iii): $T = 1$ (or) $T = \sin(2\pi X)$, $0 \leq X \leq 1$, $Y = 0$

The properties of the nanofluid are [11,12,14];

$$\rho_{nf} = (1 - \chi)\rho_f + \chi\rho_s \tag{9}$$

$$\mu_{nf} = \frac{\mu_f}{(1 - \chi)^{2.5}} \tag{10}$$

$$\alpha_{nf} = \frac{k_{eff}}{(\rho C_p)_{nf}} \tag{11}$$

$$(\rho C_p)_{nf} = (1 - \chi)(\rho C_p)_f + \chi(\rho C_p)_s \tag{12}$$

$$(\rho\beta)_{nf} = (1 - \chi)\rho_f\beta_f + \chi\rho_s\beta_s \tag{13}$$

Modified Maxwell [30] model is considered for the effective thermal conductivity, which includes the Brownian motion and it is expressed as:

$$\frac{k_{eff}}{k_f} = \frac{(k_{eq} + 2k_f) + 2(k_{eq} - k_f)(1 + \omega)^3\chi}{(k_{eq} + 2k_f) - (k_{eq} - k_f)(1 + \omega)^3\chi} \tag{14}$$

where $\omega = (h_{nl}/r_s)$ and k_{eq} is the of nanoparticles and their layers:

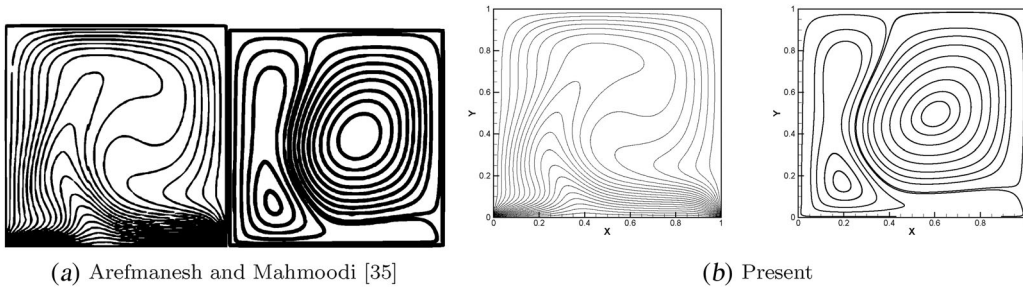


Figure 3. Comparison of isotherms and streamlines with the results of Arefmanesh and Mahmoodi [35] at $Ri = 100$, $\chi = 0.03$ and $Gr = 10^4$.

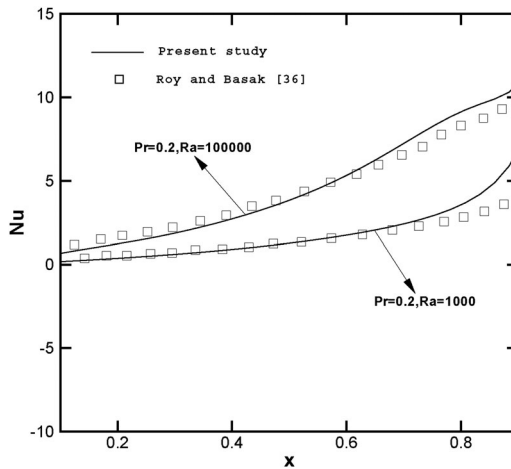


Figure 4. Comparison of the local Nusselt number with the results of Roy and Basak [36].

$$\frac{k_{eq}}{k_s} = \eta \frac{(1 + \omega)^3 (1 + 2\eta) + 2(1 - \eta)}{(1 + \omega)^3 (1 + 2\eta) - (1 - \eta)} \quad (15)$$

In this equation, $(\eta = k_{nl}/k_s)$. In the present investigation, thickness of nano-layer, radius of nanoparticles, and thermal conductivity of nano-layer are assumed to be $k_{nl} = 100k_f$, radius $r_s = 3nm$, and $h_{nl} = 2nm$. Experimentally validated the above model for the same conditions by Yu and Choi [33].

The local Nusselt number (Nu) and the average Nusselt number (Nu_{avg}) are defined by

$$Nu = -\frac{k_{eff}}{k_f} (1 + 4R/3) \left(\frac{\partial T}{\partial Y} \right)_{(Y=0)} \quad (16)$$

and

$$Nu_{avg} = \int_0^1 Nu dX. \quad (17)$$

3. Numerical solution and code verification

The nonlinear convective terms are appeared in the conservative form of governing Eqs. (5)–(8) of fluid flow. Due to the presence of these terms, it is complicated one for finding the solution of Eqs. (5)–(8) analytically. Hence, the numerical method is followed to find the solutions. Especially, FVM is adopted in this study. It can be applied to any physical (computational)

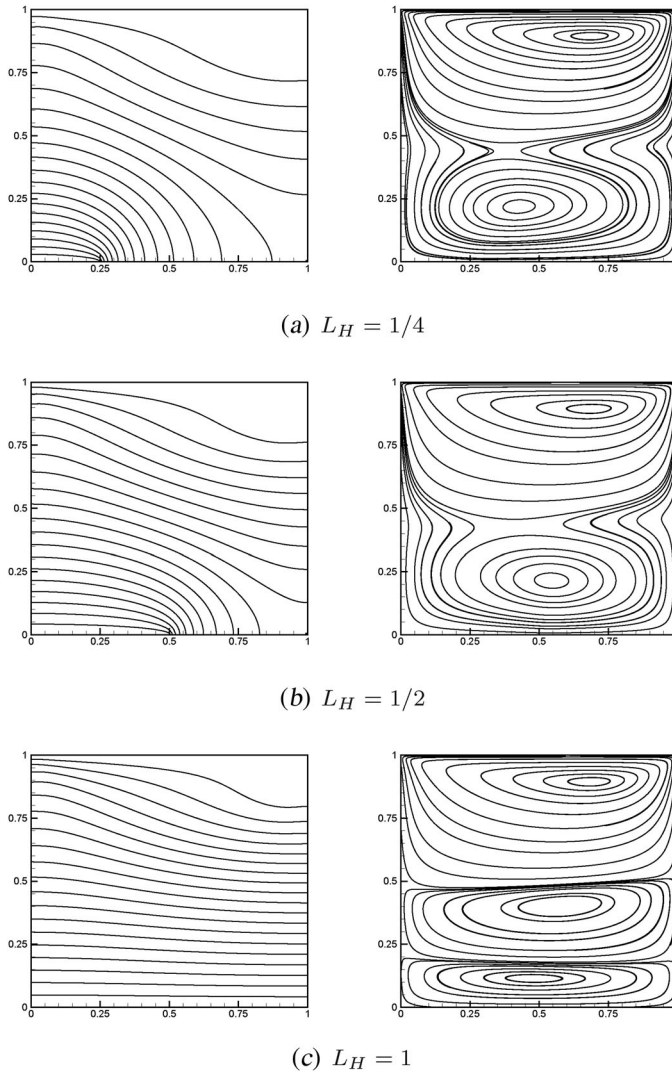


Figure 5. Isotherms and streamlines for different lengths of the heater with uniform heating at $Ri = 1$, $R = 2$, $Ha = 50$, $Da = 10^{-2}$, and $\chi = 0.06$. (a) $L_H = 1/4$; (b) $L_H = 1/2$; (c) $L_H = 1$.

domain, which is solely asymmetrical and complex, by assuming arbitrary volumes for dividing the physical domain. It is mandatory to divide the computational domain into a finite number of control volumes for applying FVM. Commonly, the accuracy of the solution and the computational time depends on the number of control volumes. Keep it in mind, the domain is divided. In an incompressible flow, there is no apparent equation for pressure term. Therefore, finding the solution of a system of equations is complex one. To overcome this issue, a uniform staggered grid is followed with pressure correction schemes. The idea of a staggered grid is to define the scalar quantities (P, T) at nodal points and vector quantities (U, V) at the cell faces of the control volume. In this method, the pressure and velocity corrections can be made simultaneously. Patankar's [34] SIMPLE algorithm is followed to combine the terms velocity and pressure. The schemes used to discretize the convection and diffusion terms are the third-order accurate deferred QUICK scheme of Hayase et al. [31] and central difference scheme, respectively. Finally, TDMA line-by-line algorithm is applied to solve the system of discretized equations. The iteration continues until the following convergence condition is fulfilled $\sum_{i,j=1}^{i_{max},j_{max}} (\Gamma_{i,j}^{n+1} - \Gamma_{i,j}^n) < 10^{-6}$,

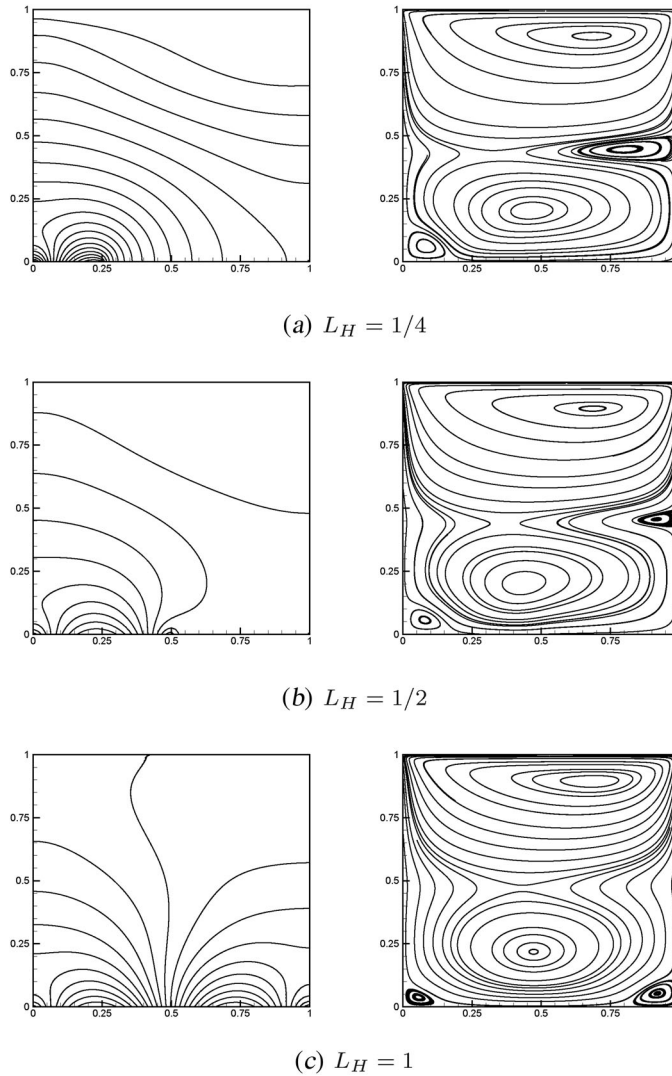


Figure 6. Isotherms and streamlines for different lengths of the heater with nonuniform heating at $Ri = 1$, $R = 2$, $Ha = 50$, $Da = 10^{-2}$, and $\chi = 0.06$.

where Γ represents U , V , P , or T . Figure 2 depicts the average Nusselt number for various grid sizes varies from 21×21 to 121×121 at $Ha = 50$, $Da = 0.01$, and $\chi = 0.06$ for both type of heaters with different lengths. In this grid sensitivity analysis, the bottom wall is considered to have a sinusoidal temperature with heater length $L_H = 1/2$. It is found that the grid size 81×81 is enough for getting the numerical results with excellent accurateness. Figures 3 and 4 compare the present numerical results with the results of Arefmanesh and Mahmoudi [35] and with the results Roy and Basak [36] for validating the developed programming code. It can be seen from Figures 3 and 4 that a great agreement between the current and the previous results exists.

4. Results and discussion

The behavior of thermal radiation and thermal source length extended along with the bottom wall from left to right in a nanofluid-filled porous cavity in the appearance of magnetic field is

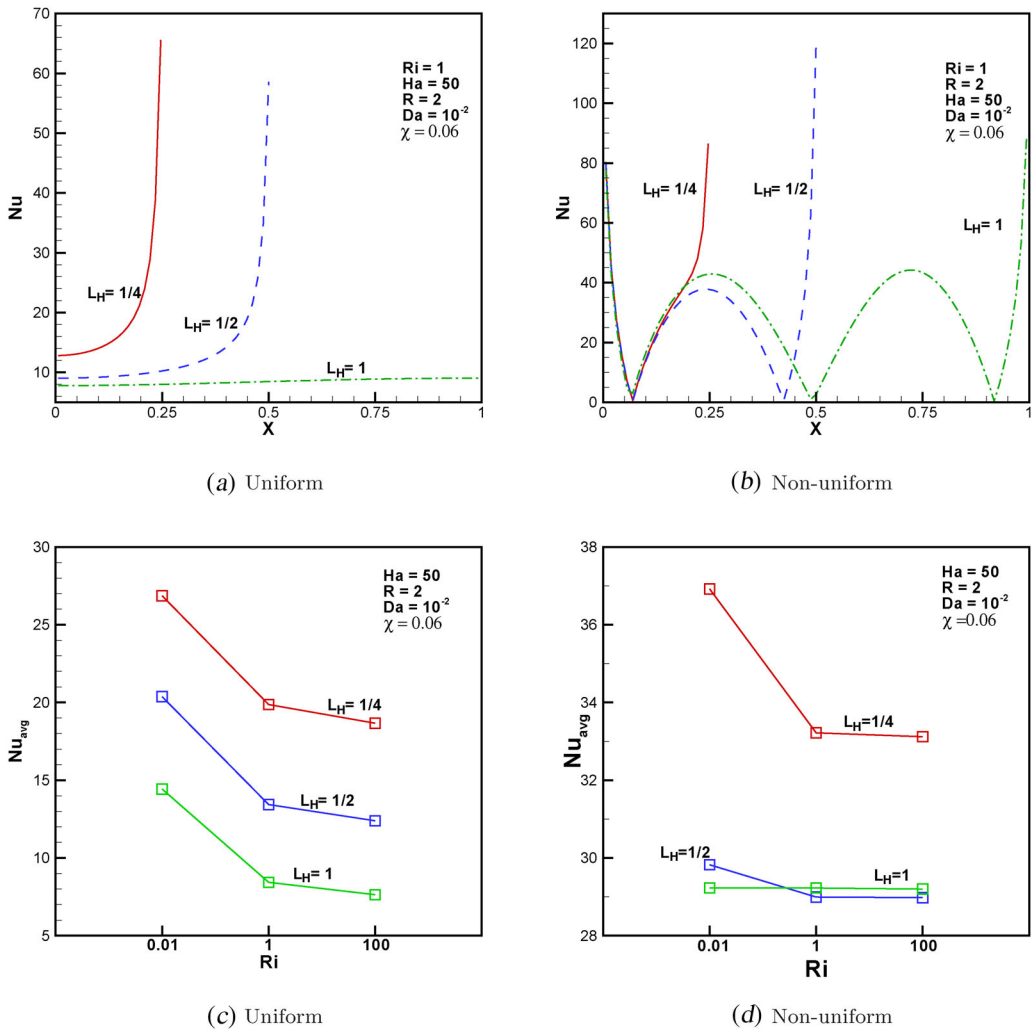


Figure 7. Local and average Nusselt numbers for different Richardson numbers and lengths of the heater at $Ha = 50$, $R = 2$, $Da = 10^{-2}$, and $\chi = 0.06$.

studied numerically. The bottom wall is heated with two different types of heater (both uniform and nonuniform) separately. Whereas, the driving top wall is kept at constant cold temperature. The rest of the bottom wall and the other walls are adiabatic. In this entire investigation, the Prandtl number of the working nanofluid is 6.2 and the porosity of the porous medium is 0.4. The different parameters related to this study are Richardson number ($0.01 \leq Ri \leq 100$), Darcy number ($0.0001 \leq Da \leq 0.1$), Radiation parameter ($0 \leq R \leq 2$), Hartmann number ($0 \leq Ha \leq 70$), and the solid volume fraction ($0.00 \leq \chi \leq 0.06$). The influences of the above parameters on fluid flow and heat transfer behavior are explained with the help of isotherms, streamlines, and local and average Nusselt numbers.

In order to discuss the impact of heater length, the other parameters are fixed as $Ri = 1$, $Da = 0.01$, $R = 2$, $Ha = 50$, and $\chi = 0.06$. Figure 5 depicts the isotherms and flow pattern with uniform heating for different L_H . When $L_H = 1/4$, the temperature contours are distributed closely near the heater and tilted kind of isotherms are distributed almost in the whole chamber. A binary eye pattern clockwise rotating (CW) vortex exists inside the cavity. When increasing the heater length to $1/2$ and to 1 , the slanted isotherms are nearly changed into straight line form. It

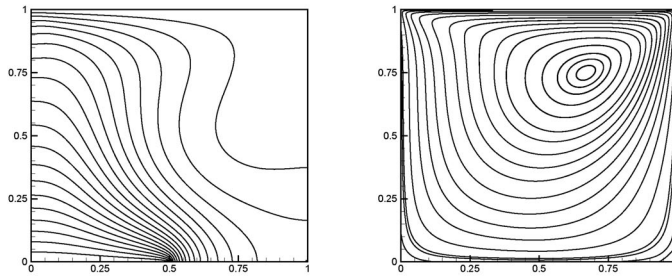
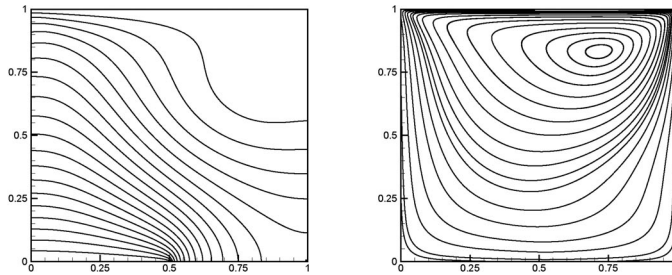
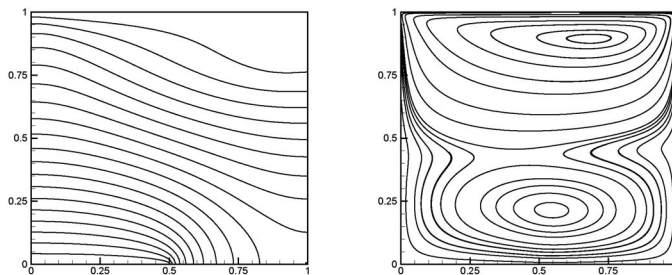
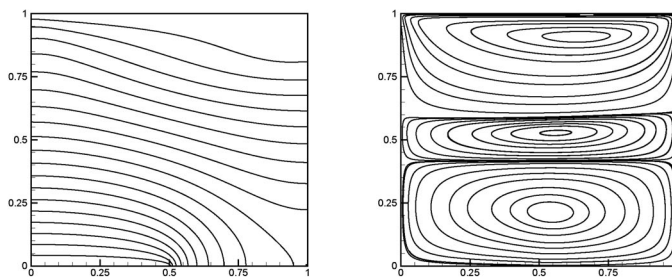
(a) $Ha = 0$ (b) $Ha = 20$ (c) $Ha = 50$ (d) $Ha = 70$

Figure 8. Isotherms and streamlines for different Hartmann numbers with uniform heating at $Ri = 1$, $R = 2$, $L_H = 1/2$, $Da = 10^{-2}$, and $\chi = 0.06$. (a) $Ha = 0$; (b) $Ha = 20$; (c) $Ha = 50$; (d) $Ha = 70$.

is noticed that there is no change in the flow type when expanding the heater length to $L_H = 1/2$. Further, when $L_H = 1$, the existing flow behavior is entirely affected and three cell flow

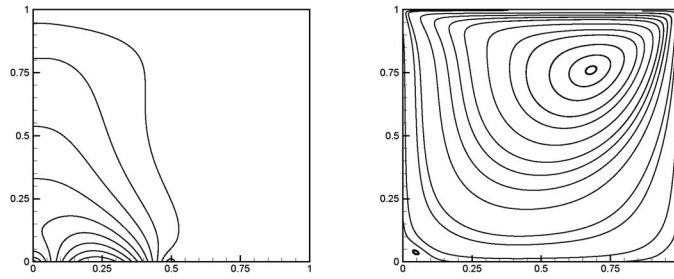
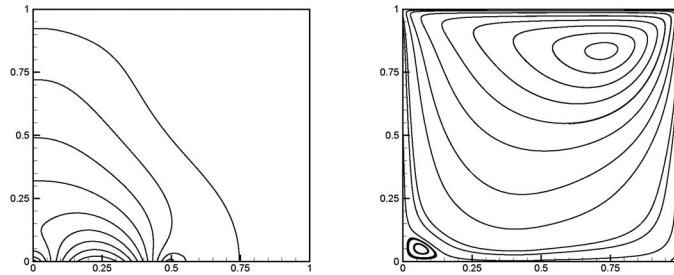
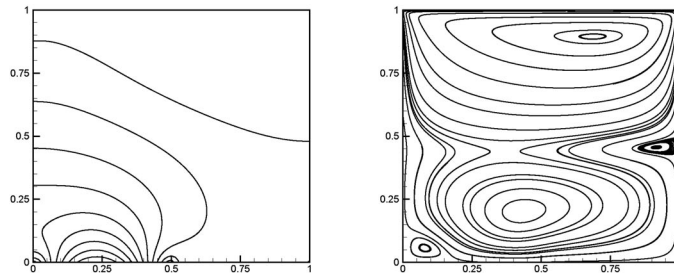
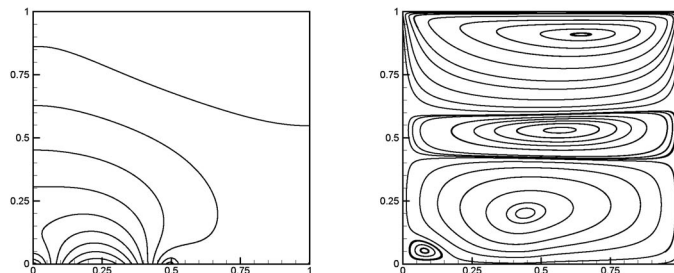
(a) $Ha = 0$ (b) $Ha = 20$ (c) $Ha = 50$ (d) $Ha = 70$

Figure 9. Isotherms and streamlines for different Hartmann numbers with nonuniform heating at $Ri = 1$, $R = 2$, $L_H = 1/2$, $Da = 10^{-2}$, and $\chi = 0.06$.

pattern is appeared. Figure 6 reports the changes in streamlines and isotherms with respect to thermal source length with nonuniform heating. For $L_H = 1/4$, a thin thermal boundary layer is

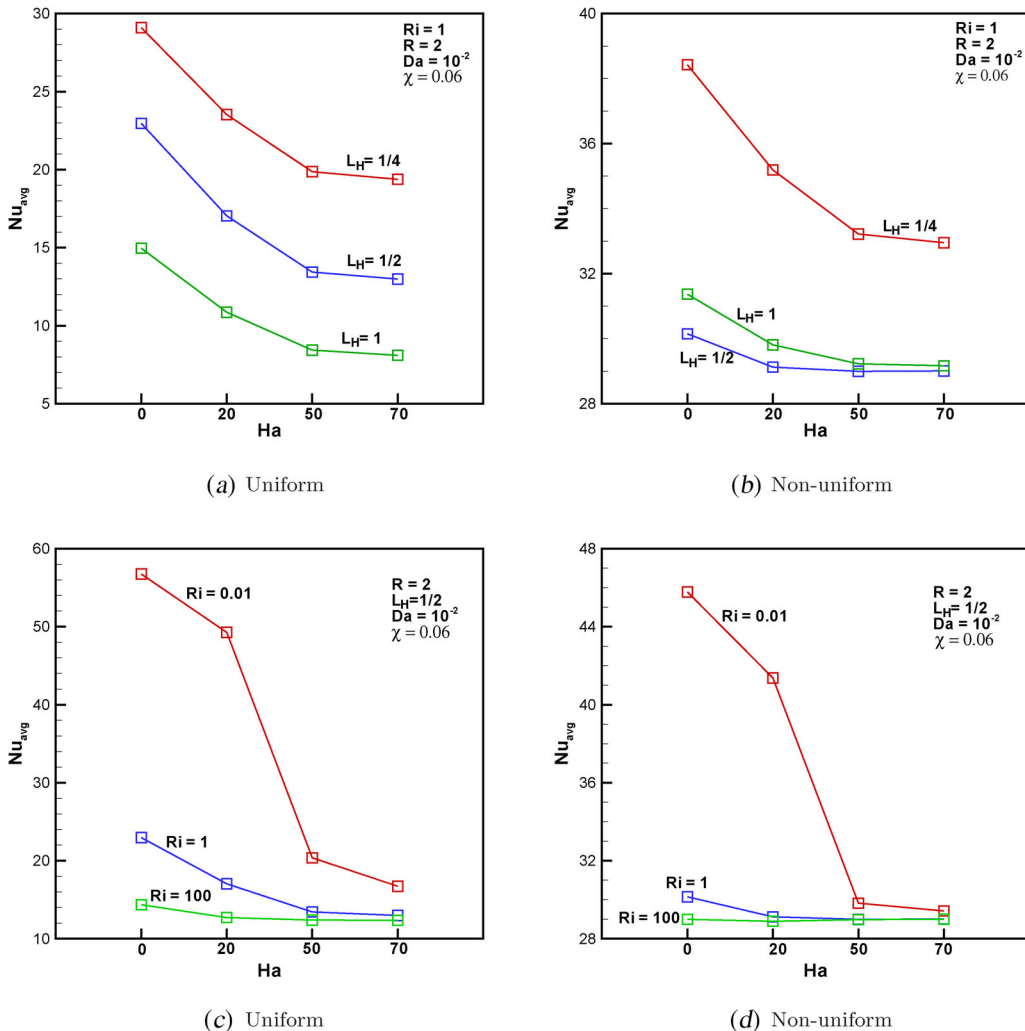


Figure 10. Average Nusselt numbers for different Hartmann numbers, length of heater, and Richardson numbers at $R = 2$, $Da = 10^{-2}$, and $\chi = 0.06$.

formed at lower left corner of the cell. A primary vortex with two core points, a secondary vortex at mid-section of the right part of the enclosure and a little eddy exists at the bottom left corner of the chamber. When $L_H = 1/2$, the isotherms are distributed at the left side of the enclosure. That is, the fluid temperature changes significantly at the left half of the enclosure. The secondary cell size reduces. For $L_H = 1$, thermal boundary layer is formed along the entire heater. Since the right part of the bottom wall is cooled the secondary cell disappears and a new cell appears at right bottom corner. Figure 7 demonstrates the local and average Nusselt numbers with various heater lengths and Richardson number. In the case of uniform heating, the local Nusselt number curve starts with lowest value at left side wall and attains its highest value at the end of thermal source for $L_H = 1/4$ and $L_H = 1/2$. Whereas it has almost equal value throughout the entire bottom wall with $L_H = 1$ due to the straightened behavior happened in isotherms. For nonuniform heating, the local Nusselt number curve reflects the heating behavior of the thermal source for all the considered lengths. A linear decrement can be observed in Nu_{avg} with an augmentation in either L_H or Ri with uniform temperature. In the case of sinusoidal heating, mean Nusselt number is reduced with a rise in L_H at $Ri = 0.01$ for the same incident it is reduced first and then increased slightly at $Ri = 1$.

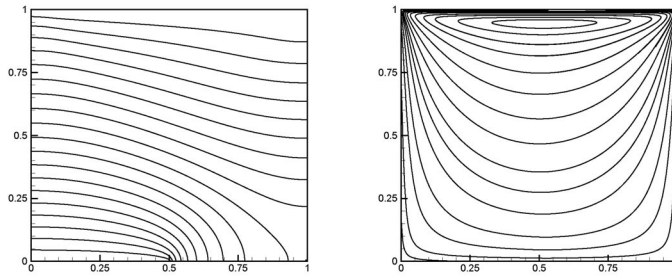
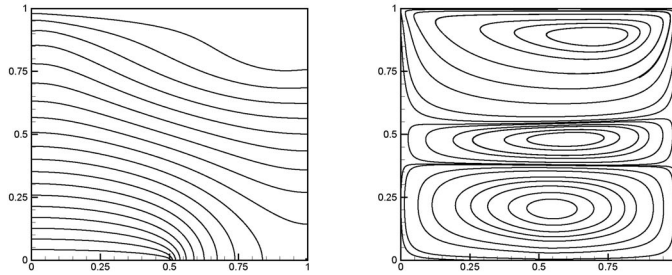
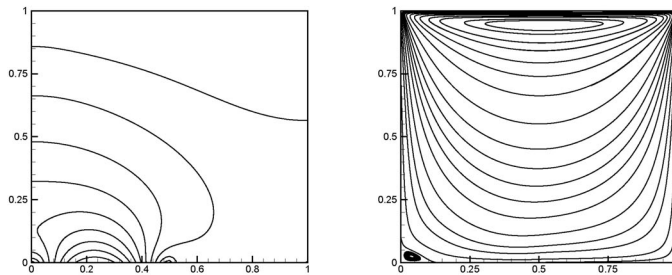
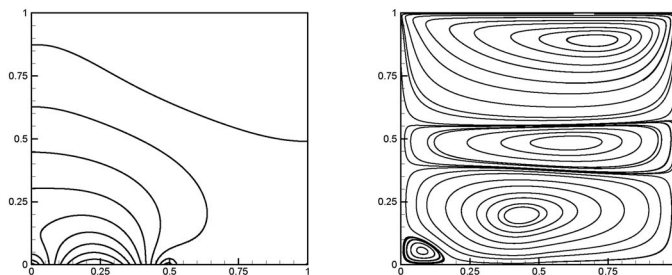
(a) $Da = 0.0001$ (b) $Da = 0.1$ (c) $Da = 0.0001$ (d) $Da = 0.1$

Figure 11. Isotherms and streamlines for different Darcy numbers with (a,b) uniform heating and (c,d) nonuniform heating at $Ri = 1$, $R = 2$, $L_H = 1/2$, $Ha = 50$, and $\chi = 0.06$.

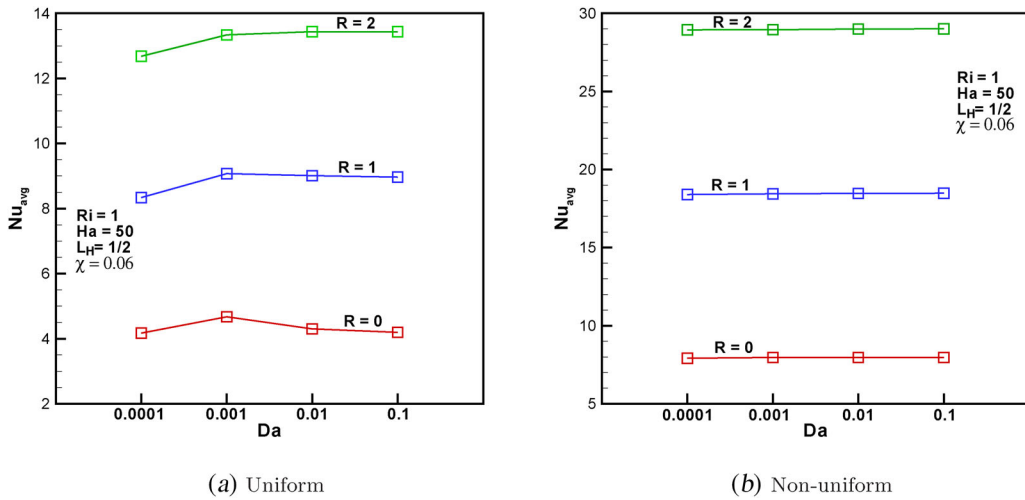


Figure 12. Average Nusselt numbers for different Darcy numbers and radiation parameters at $Ri = 1$, $L_H = 1/2$, $Ha = 50$, and $\chi = 0.06$.

The effect of Ha is analyzed with the fixed value of $Ri = 1$, $L_H = 1/2$, $R = 2$, $Da = 0.01$, and $\chi = 0.06$. Streamlines and isotherms for various Ha with uniform heating are presented in Figure 8. For $Ha = 0$, the isotherms resemble convection is the code of heat transfer within the chamber and the cavity is filled with CW circulating vortex. While increasing Ha , convection gets change into conduction and tricellular flow structure replaces the single vortex. The reason for this behavior is Laurentz force caused by the magnetic field. This is a resistive force and drage the fluid particles from its movement. In Figure 9, the temperature distributions and fluid flow patterns with increase of Ha is depicted. Sinusoidal thermal source with heating part is alone considered at left half of the bottom wall. For $Ha = 0$, the isotherm contours are packed closely near the heating portion and also distributed at the left half of the enclosure. The heat is transferred more dynamically in the left side than the right side. The fluid particles are moved in CW direction and form a single vortex. Also a tiny cell near the left corner of the cavity appears. When the Lorentz force is applied and increased significantly, the distributions of isotherms are changed. CW direction cell is broken into three cells and rotate one on the above other in opposite directions. The mean Nusselt number for various L_H , Ri versus Ha is plotted in Figure 10. For all considered heater length and nature, an enhancement in Ha leads to reduce the heat transfer. In the case of sinusoidal thermal heating, Nu_{avg} is decreased initially and then raised on lengthening the heater size whereas; it is diminished linearly in uniform heating. When $Ha = 0$ and 20, the Nu_{avg} is maximum in uniform heating than sinusoidal heating. Otherwise, nonuniform heating enhances the heat transfer. Regardless of the nature of thermal source, Nu_{avg} is reduced with respect to augment in either magnetic field parameter or Ri .

The effect of the Darcy number on the flow pattern and isotherms are shown in Figure 11 for the fixed value of $Ha = 50$, $Ri = 1$, $R = 2$, $L_H = 1/2$, and $\chi = 0.06$. Increasing the Da in the presence of magnetic field and thermal radiation does not affect the distribution of isotherms for both type of heating. At low Da , a CW vortex exists inside the chamber. Whereas it is broken into three vortices when increasing Da . This behavior is happened due to the increase of permeability of porous medium. In other words, at high permeability of porous medium, the fluid particles can move freely inside the cavity whereas it is restricted to move at low permeability of porous medium. It is observed from Figure 12, which displays the thermal radiation effect versus the Da on average Nusselt number, a rise in the thermal radiation enhances the heat transfer rate significantly for all the taken Da and the heating source. The impact of thermal radiation is significant on increasing Darcy number in uniform heating than sinusoidal heating. Figure 13 shows

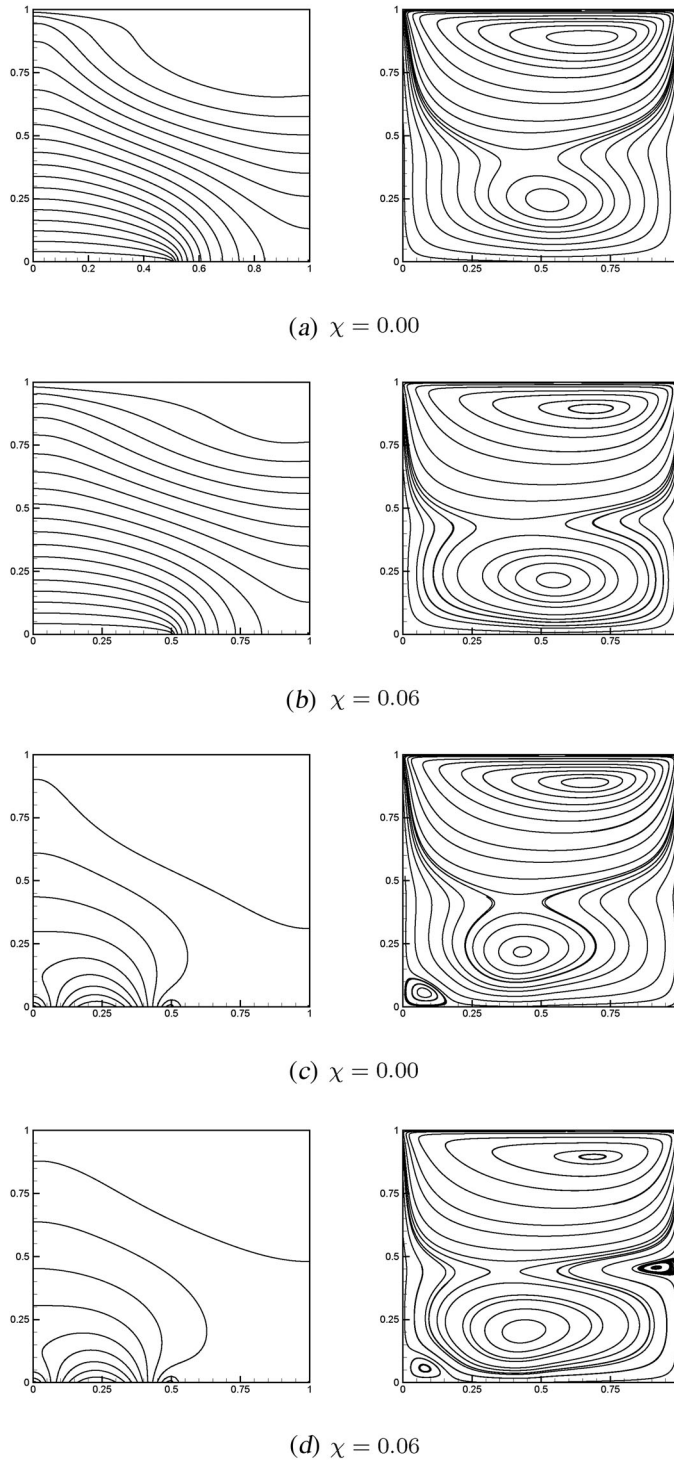


Figure 13. Isotherms and streamlines for different solid volume fractions with (a,b) uniform heating and (c,d) nonuniform heating at $Ri = 1$, $R = 2$, $L_H = 1/2$, $Ha = 50$ and $Da = 0.01$.

the isotherms and streamlines at $Ri = 1$, $R = 2$, $Ha = 50$, $Da = 0.01$, and $L_H = 1/2$ for pure fluid and nanofluid with uniform and nonuniform heating. When $\chi = 0.00$, the temperature

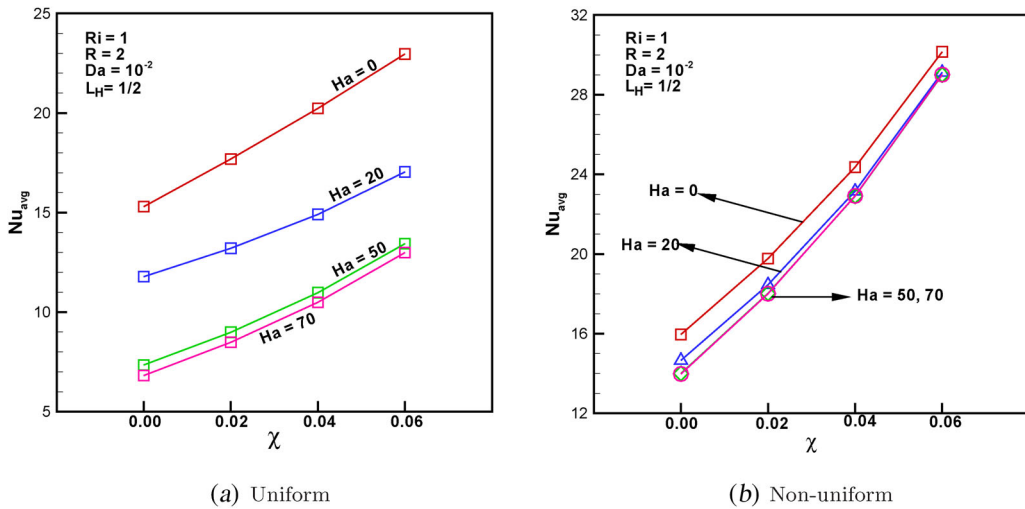


Figure 14. Average Nusselt numbers for different solid volume fractions and Hartmann numbers at $Ri = 1$, $L_H = 1/2$, $R = 2$, and $Da = 0.02$.

contours are distributed throughout the cavity and streamlines show that the fluid flow happens in a CW rotating vortex with two kernels in uniform heating. On increasing the χ value the flow pattern and temperature distribution are almost same. This behavior can be noticed from Figure 13a, b. In the case of pure fluid or nanofluid, isotherms are more active on the left part of the cavity with sinusoidal heating. A secondary cell is formed near the middle of right wall when increasing the percentage of solid and volume. The changes in Nu_{avg} with respect to Ha and χ are displayed in Figure 14. For both type of heating and all considered Ha , a linear increment can be noticed in Nu_{avg} with an increase of percentage of solid volume. Further sinusoidal heating enhance the heat transfer rate than uniform heating. Significant effect on heat transfer rate is noticed with an increase of Ha for all considered solid volume fraction in uniform heating.

5. Conclusions

The behavior of thermal radiation and thermal source length extended along the bottom wall from left to right in a nanofluid-filled porous cavity in the appearance of magnetic field is studied numerically. The following conclusions have been drawn from the simulation results;

- Regardless of the heating nature, the heat transfer is maximum with the length of heater $L_H = 1/4$ for all taken Richardson number. In the case of Sinusoidal heating, the average Nusselt number gets its low value at $Ri = 0.01$ with $L_H = 1$. Whereas, it is minimum at $Ri = 1$ and 100 with $L_H = 1/2$.
- In any case of length of the heater, nonuniform heating produces improved heat transfer rate than uniform heating.
- In natural convection regime, magnetic field effect is observed at low level with the thermal source length $L_H = 1/2$ and nonuniform heating.
- In the case of sinusoidal heating, mean Nusselt number is decreased initially and then raised on lengthening the heater size whereas it is diminished linearly in uniform heating.
- The impact of thermal radiation is significant on increasing Darcy number in uniform heating than sinusoidal heating. A rise in the thermal radiation increases the average Nusselt number significantly for all the taken Da and the heating source.

- For all considered solid volume fraction, the magnetic field changes the heat transfer rate significantly in uniform heating than nonuniform heating.

Disclosure statement

The authors declare that they have no known competing financial interests or personal relationships that could have appeared to influence the work reported in this paper.

Funding

This research was funded by the Princess Nourah bint Abdulrahman University Researchers Supporting Project (PNURSP2022R154), Princess Nourah bint Abdulrahman University, Riyadh, Saudi Arabia.

References

- [1] H. F. Oztop, K. Al-Salem and I. Pop, "MHD mixed convection in a lid-driven cavity with corner heater," *Int. J. Heat Mass Transf.*, vol. 54, no. 15-16, pp. 3494–3504, Jul. 2011. DOI: [10.1016/j.ijheatmasstransfer.2011.03.036](https://doi.org/10.1016/j.ijheatmasstransfer.2011.03.036).
- [2] M. M. K. Dawood and M. A. Teamah, "Hydro-magnetic mixed convection double diffusive in a lid driven square cavity," *Eur. J. Sci. Res.*, vol. 85, no. 3, pp. 336–355, Sep. 2012.
- [3] S. Ray and D. Chatterjee, "MHD mixed convection in a lid-driven cavity including heat conducting circular solid object and corner heaters with Joule heating," *Int. Comm. Heat Mass Transf.*, vol. 57, pp. 200–207, Oct. 2014. DOI: [10.1016/j.icheatmasstransfer.2014.07.029](https://doi.org/10.1016/j.icheatmasstransfer.2014.07.029).
- [4] A. Malleswaran and S. Sivasankaran, KS Rangasamy College of Technology "A numerical simulation on MHD mixed convection in a lid-driven cavity with corner heaters," *J. Appl. Fluid Mech.*, vol. 9, no. 1, pp. 311–319, Jan. 2016. DOI: [10.18869/acadpub.jafm.68.224.22903](https://doi.org/10.18869/acadpub.jafm.68.224.22903).
- [5] F. Selimefendigil and A. J. Chamkha, "Magnetohydrodynamics mixed convection in a lid-driven cavity having a corrugated bottom wall and filled with a non-Newtonian power-law fluid under the influence of an inclined magnetic field," *J. Therm. Sci. Eng. Appl.*, vol. 8, no. 2, pp. 021023, Jun. 2016. DOI: [10.1115/1.4032760](https://doi.org/10.1115/1.4032760).
- [6] M. A. Ismael, I. Pop and A. J. Chamkha, "Mixed convection in a lid-driven square cavity with partial slip," *Int. J. Ther. Sci.*, vol. 82, pp. 47–61, Aug. 2014. DOI: [10.1016/j.ijthermalsci.2014.03.007](https://doi.org/10.1016/j.ijthermalsci.2014.03.007).
- [7] M. A. Ismael and A. J. Chamkha, "Mixed convection lid0driven trapezoidal cavities with an aidind and opposing side wall" *Num. Heat Trans. A*, vol. 68, no. 3, pp. 312–335, Apr. 2015. DOI: [10.1080/10407782.2014.986001](https://doi.org/10.1080/10407782.2014.986001).
- [8] S. U. S. Choi and J. A. Eastman, "Enhancing thermal conductivity of fluids with nanoparticles," *ASME Fluids Eng. Div.*, vol. 231, pp. 99–105, Oct. 1995.
- [9] C. H. Chon and K. D. Kihm, "Empirical correlation finding the role of temperature and particle size for nanofluid Al_2O_3 thermal conductivity enhancement," *App. Phys. Lett.*, vol. 87, pp. 153107, Apr. 2005. DOI: [10.1063/1.2093936](https://doi.org/10.1063/1.2093936).
- [10] C. T. Nguyen, et al., "Temperature and particle-size dependent viscosity data for water-based nanofluids – Hysteresis phenomenon," *Int. J. Heat Fluid Flow*, vol. 28, no. 6, pp. 1492–1506, Dec. 2007. DOI: [10.1016/j.ijheatfluidflow.2007.02.004](https://doi.org/10.1016/j.ijheatfluidflow.2007.02.004).
- [11] M. H. Esfe, A. Z. Ghadi and M. J. Noroozi, "Numerical simulation of mixed convection within nanofluid-filled cavities with two adjacent moving walls," *Trans. Can. Soc. Mech. Eng.*, vol. 37, no. 4, pp. 1073–1089, Dec. 2013. DOI: [10.1139/tcsme-2013-0092](https://doi.org/10.1139/tcsme-2013-0092).
- [12] H. Salahi, M. A. R. Sharif and S. Rasouli, "Laminar mixed convective heat transfer in a shallow inclined lid-driven cavity filled with nanofluid," *J. Therm. Sci. Eng. Appl.*, vol. 7, no. 4, pp. 041016–1-13, Dec. 2015. DOI: [10.1115/1.4031221](https://doi.org/10.1115/1.4031221).
- [13] F. Selimefendigil and H. F. Oztop, "Modeling and optimization of MHD mixed convection in a lid-driven trapezoidal cavity filled with alumina–water nanofluid: Effects of electrical conductivity models," *Int. J. Mech. Sci.*, vol. 136, pp. 264–278, Feb. 2018. DOI: [10.1016/j.ijmecsci.2017.12.035](https://doi.org/10.1016/j.ijmecsci.2017.12.035).
- [14] S. E. Ahmed, et al., "MHD mixed convection in an inclined cavity containing adiabatic obstacle and filled with Cu–water nanofluid in the presence of the heat generation and partial slip," *J. Therm. Anal. Calorim.*, vol. 138, no. 2, pp. 1443–1460, May 2019. DOI: [10.1007/s10973-019-08340-3](https://doi.org/10.1007/s10973-019-08340-3).

- [15] M. A. Ismael, E. Abu-Nada and A. J. Chamkha, "Mixed convection in a square cavity filled with CuO-water nanofluid heated by corner heater," *Int. J. Mech. Sci.*, vol. 133, pp. 42–50, Aug. 2017. DOI: [10.1016/j.jmecs.2017.08.029](https://doi.org/10.1016/j.jmecs.2017.08.029).
- [16] P. Barnoon, D. Toghraie, R. B. Dehkordi and H. Abedb, "MHD mixed convection and entropy generation in a lid-driven cavity with rotating cylinders filled by a nanofluid using two phase mixture model," *J. Magn. Magn. Mater.*, vol. 483, pp. 224–248, Aug. 2019. DOI: [10.1016/j.jmmm.2019.03.108](https://doi.org/10.1016/j.jmmm.2019.03.108).
- [17] M. M. Irwan, A. M. Fudhail, C. N. Azwadi and G. Masoud, "Numerical investigation of incompressible fluid flow through porous media in a lid-driven square cavity," *Am. J. Appl. Sci.*, vol. 7, no. 10, pp. 1341–1344, Jan. 2010. DOI: [10.3844/ajassp.2010.1341.1344](https://doi.org/10.3844/ajassp.2010.1341.1344).
- [18] D. Ramakrishna, T. Basak, S. Roy and I. Pop, "Numerical study of mixed convection within porous square cavities using Bejan's heatlines: effects of thermal aspect ratio and thermal boundary conditions," *Int. J. Heat Mass Trans.*, vol. 55, no. 21–22, pp. 5436–5448, Oct. 2012. DOI: [10.1016/j.ijheatmasstransfer.2012.04.058](https://doi.org/10.1016/j.ijheatmasstransfer.2012.04.058).
- [19] Y. Wang and G. Qin, "Accurate numerical simulation for non-Darcy double-diffusive mixed convection in a double lid-driven porous cavity using SEM," *Num. Heat. Transf. Part A. Appl.*, vol. 75, no. 9, pp. 598–615, Apr. 2019. DOI: [10.1080/10407782.2019.1608764](https://doi.org/10.1080/10407782.2019.1608764).
- [20] M. A. Mansour, et al., "MHD mixed bioconvection in a square porous cavity filled by gyrotactic micro-organisms," *Int. J. Heat Technol.*, vol. 37, no. 2, pp. 433–445, Jun. 2019. DOI: [10.18280/ijht.370209](https://doi.org/10.18280/ijht.370209).
- [21] M. A. Hossain, M. A. Saleem, S. C. Saha and A. Nakayama, "Conduction-radiation effect on natural convection flow in fluid-saturated non-Darcy porous medium enclosed by non-isothermal walls," *Appl. Math. Mech. Engl. Ed.*, vol. 34, no. 6, pp. 687–702, Jun. 2013. DOI: [10.1007/s10483-013-1700-7](https://doi.org/10.1007/s10483-013-1700-7).
- [22] S. E. Ahmed, et al., "Viscous dissipation and radiation effects on MHD natural convection in a square enclosure filled with a porous medium," *Nucl. Eng. Des.*, vol. 266, pp. 34–42, Jan. 2014. DOI: [10.1016/j.nucengdes.2013.10.016](https://doi.org/10.1016/j.nucengdes.2013.10.016).
- [23] C. Sivaraj and M. A. Sheremet, "Natural convection coupled with thermal radiation in a square porous cavity having a heated plate inside," *Transp. Porous Med.*, vol. 114, no. 3, pp. 843–857, Sep. 2016. DOI: [10.1007/s11242-016-0747-2](https://doi.org/10.1007/s11242-016-0747-2).
- [24] M. Bibi, A. Zeeshan and M. Y. Malik, "Numerical analysis of unsteady flow of three-dimensional Williamson fluid-particle suspension with MHD and nonlinear thermal radiations," *The Eur. Phys. J. Plus*, vol. 135, no. 850, pp. 1–26, Oct. 2020. DOI: [10.1140/epjp/s13360-020-00857-z](https://doi.org/10.1140/epjp/s13360-020-00857-z).
- [25] A. K. Ray, et al., "Convective Flow of Non-homogeneous Fluid Conveying Nano-Sized Particles with Non-Fourier Thermal Relaxation: Application in Polymer Coating," *Arab J. Sci. Eng.*, vol. 47, no. 5, pp. 6559–6576, Jan. 2022. DOI: [10.1007/s13369-021-06467-w](https://doi.org/10.1007/s13369-021-06467-w).
- [26] T. Javed, Z. Mehmood and M. A. Siddiqui, "Mixed convection in a triangular cavity permeated with micropolar nanofluid-saturated porous medium under the impact of MHD," *J. Braz. Soc. Mech. Sci. Eng.*, vol. 39, no. 10, pp. 3897–3909, Jul. 2017. DOI: [10.1007/s40430-017-0850-5](https://doi.org/10.1007/s40430-017-0850-5).
- [27] H. Babazadeh, A. Zeeshan, K. Jacob, A. Hajizadeh and M. M. Bhatti, "Numerical modelling for nanoparticle thermal migration with effects of shape of particles and magnetic field inside a porous enclosure," *Iran J. Sci. Technol. Trans. Mech. Eng.*, vol. 45, no. 3, pp. 801–811, Feb. 2021. DOI: [10.1007/s40997-020-00354-9](https://doi.org/10.1007/s40997-020-00354-9).
- [28] A. Riaz, A. Zeeshan, M. M. Bhatti and R. Ellahib, "Peristaltic propulsion of Jeffrey nano-liquid and heat transfer through a symmetrical duct with moving walls in a porous medium," *Phys. A Stat. Mech. Appl.*, vol. 545, pp. 123788, May 2020. DOI: [10.1016/j.physa.2019.123788](https://doi.org/10.1016/j.physa.2019.123788).
- [29] A. M. Aly, Z. A. S. Raizah and M. Sheikholeslami, "Analysis of mixed convection in a sloshing porous cavity filled with a nanofluid using ISPH method," *J. Therm. Anal. Calorim.*, vol. 139, no. 3, pp. 1977–1991, Jul. 2020. DOI: [10.1007/s10973-019-08575-0](https://doi.org/10.1007/s10973-019-08575-0).
- [30] J. C. Maxwell, *A Treatise on Electricity and Magnetism*, Vol. 1. London: Clarendon Press, 1873.
- [31] T. Hayase, J. A. C. Humphrey and R. Greif, "A consistently formulated QUICK scheme for fast and stable convergence using finite-volume iterative calculation procedures," *J. Comput. Phys.*, vol. 98, no. 1, pp. 108–118, Jan. 1992. DOI: [10.1016/0021-9991\(92\)90177-Z](https://doi.org/10.1016/0021-9991(92)90177-Z).
- [32] S. Ergun, "Fluid flow through packed columns," *Chem. Eng. Prog.*, vol. 48, pp. 89–94, Feb. 1952.
- [33] W. Yu and S. U. S. Choi, "The role of interfacial layers in the enhanced thermal conductivity of nanofluids: a renovated Maxwell model," *J. Nanopart. Res.*, vol. 5, no. 1/2, pp. 167–171, Apr. 2003. DOI: [10.1023/A:1024438603801](https://doi.org/10.1023/A:1024438603801).
- [34] S. V. Patankar, *Numerical Heat Transfer and Fluid Flow*. Washinton, DC: Hemisphere, 1980.
- [35] A. Arefmanesh and M. Mahmoodi, "Effects of uncertainties of viscosity models for Al_2O_3 -water nanofluid on mixed convection numerical simulations," *Int. J. Ther. Sci.*, vol. 50, no. 9, pp. 1706–1719, Sep. 2011. DOI: [10.1016/j.ijthermalsci.2011.04.007](https://doi.org/10.1016/j.ijthermalsci.2011.04.007).
- [36] S. Roy and T. Basak, "Finite element analysis of natural convection flows in a square cavity with non-uniformly heated wall(s)," *Int. J. Eng. Sci.*, vol. 43, no. 8–9, pp. 668–680, May 2005. DOI: [10.1016/j.jengsci.2005.01.002](https://doi.org/10.1016/j.jengsci.2005.01.002).